Available online at www.sciencedirect.com
ScienceDirect
Applied Catalysis B: Environmental 82 (2008) 208–218
APPLIED CATALYSIS B: ENVIRONMENTAL
www.elsevier.com/locate/apcatb

Preparation and photocatalytic activity of hierarchically mesoporous-macroporous $TiO_{2-x}N_x$

Gao-Song Shao, Xue-Jun Zhang, Zhong-Yong Yuan *

Institute of New Catalytic Materials Science, Engineering Research Center of Energy Storage and Conversion (Ministry of Education), College of Chemistry, Nankai University, Tianjin 300071, PR China

Received 25 August 2007; received in revised form 10 January 2008; accepted 26 January 2008
Available online 7 February 2008

Abstract

Hierarchically mesoporous-macroporous N-doped titania materials were fabricated by the thermal treatment of spontaneously formed hierarchical mesoporous-macroporous titanias with urea solution, in order to extend their photocatalytic applications from ultraviolet to visible-light range. The resultant meso-macroporous $TiO_{2-x}N_x$ exhibited a bicrystalline (anatase and brookite) framework with high surface area and large porosity. The content of the doped nitrogen increased with the urea solution and the nitridation temperature, and the band gaps narrowed from 3.14 to 2.48 eV. The formation of O–Ti–N bonds in the meso-macroporous $TiO_{2-x}N_x$ was confirmed by the XPS and FT-IR spectra. The photocatalytic activity was evaluated by the photodegradation of methyl orange and rhodamine B under UV and visible-light irradiation, respectively. The significant improvement of photocatalytic activity for water contaminant decomposition under both UV and visible-light irradiation was observed, which is due to the incorporation of nitrogen into the titania lattice and the presence of the hierarchical meso-macroporous structure.

Keywords: Mesoporous-macroporous; Titanium dioxide; N-doping; Photocatalyst; Visible-light

1. Introduction

Titanium oxide is a multifunctional material with a wide variety of potential uses including catalytic applications. Much attention has been paid to TiO_2 as an efficient photocatalyst for environmental remediation and energy conversion purposes [1–3]. However, the bandgap of this material, around 3.0 eV for rutile and 3.2 eV for anatase, allows only absorption of the ultraviolet part of the solar irradiation. Many efforts have then recently been employed to develop a new material system that can effectively utilize the dominant visible-light irradiation in solar spectrum. TiO_2 photocatalysts doped with either anions (dopant = N [4–6], C [7], S [8], F [9], P [10], I [11], etc.) or cations (dopant = Fe [12], Cr [13], Mn [14], Ce [15], Ni [16], etc.) or co-doped with several ions [17–19] were reported to show their absorption edge red-shifted to lower energies (longer wavelengths), enhancing photocatalytic efficiencies in the visible-light range, though the mechanism of red-shifting of the TiO_2 absorption onset to the visible region by substitutional doping is still under debate. Substitutional N-doping was found to be particularly effective in absorption in the visible region, due to narrowing the band gap of anatase through the mixing of N and O 2p states [5]. Several methods were reported for the doping of TiO_2 with nitrogen, and considerable success has been achieved in decreasing the band gap and increasing the photocatalytic activity [4–6,20–23].

Porous and high-surface-area titania materials are of great interest for their potential in improving photocatalytic activity. Mesoporous titania with crystalline framework [24–28], even mesoporous doped TiO_2 photocatalysts [12,29–31], were synthesized, exhibiting good photocatalytic performance. Furthermore, incorporation of macropores in mesoporous materials has been demonstrated to show enhanced properties compared with single-sized pore materials due to increased mass transport through the material and maintenance of a specific surface area on the level of fine pore systems [32]. The combination of surfactant templating with micromolding technologies using latex spheres [33,34], emulsion droplets [35], starch gel [36], polymer foams [37], or the self-assembly of one single surfactant [38], renders the formation of

* Corresponding author. Tel.: +86 22 23509610; fax: +86 22 23509610.
E-mail address: zyyuan@nankai.edu.cn (Z.-Y. Yuan).

0926-3373/$ – see front matter © 2008 Elsevier B.V. All rights reserved.
doi:10.1016/j.apcatb.2008.01.026

hierarchically mesoporous-macroporous titanium dioxides (MMTD). The enhancement of photocatalytic activity of meso-macroporous titania was observed due to the increasing photoabsorption efficiency and efficient diffusion of molecules caused by the macropores [38]. Although the macroporous channels could serve as light-transfer paths for the distribution of photon energy onto the large surface of inner photoactive mesoporous frameworks, substitutional doping in the meso-macroporous titania for the improvement of visible-light photocatalytic activity has not yet been reported to date. In this work, nitrogen-doped titania with hierarchical meso-macroporous structure was prepared as active visible-light photocatalyst by nitridation of template-free synthesized meso-macroporous titania using urea as a nitrogen donor. The resultant meso-macroporous $TiO_{2-x}N_x$ was characterized by X-ray diffraction, N_2 adsorption–desorption analysis, scanning and transmission electron microscopy, FT-IR, XPS and diffuse reflectance spectroscopy. The improved photocatalytic activity was observed in the meso-macroporous $TiO_{2-x}N_x$ evaluated by the photodegradation of dye molecules under both UV and visible-light irradiation, in comparison to the undoped MMTD.

2. Experimental

2.1. Catalyst preparation

All chemicals were used as received, without further purification. The preformed MMTD was prepared by dropwise addition of tetrabutyl titanate (Kermel, AR) into the sulfuric acid solution (pH 2) and slowly stirring at room temperature until the titanium *n*-alkoxide hydrolyzed completely. The mixture was transferred into Teflon-lined autoclave and heated statically at 60 °C for two days, followed by the precipitate collection, washing and drying at 60 °C.

To fabricate the nitrogen-doped TiO_2, 2 g of the preformed MMTD powder was mixed with 5 ml of urea aqueous solution (1 or 2 mol/L), and slowly and magnetically stirred at room temperature for 5 h. The mixture was kept at room temperature for 48 h, and then washed with very diluted sulfuric acid and deionized water, and dried at 60 °C in air. Finally the obtained white powers were calcined at 350–550 °C for 1 h. The resulted N-doped TiO_2 samples are denoted as N-T-*x*/*y*, where *x* represents the concentration of urea solution used, and *y* represents the calcination temperature.

2.2. Characterization

X-ray diffraction (XRD) patterns were collected on a Rigaku D/max-2500 diffractometer with Cu K_α radiation operated at 40 kV and 100 mA.

N_2 adsorption–desorption isotherms were recorded on a Quantachrome NOVA 2000e sorption analyzer at liquid nitrogen temperature (77 K). The samples were degassed at 200 °C overnight prior to the measurement. The surface area was obtained by the Brunauer–Emmett–Teller (BET) method, and pore size distribution was calculated from the adsorption branch of the isotherm by the Barret–Joyner–Halenda (BJH) model.

Scanning electron microscopy (SEM) was taken on a Shimadzu SS-550 microscope at 15 keV. Transmission electron microscopy (TEM) was carried out on a Philips Tecnai G20 microscope, working at 200 kV. A trace amount of sample was dispersed in ethanol solution by sonication for 10 min, and then deposited on a carbon-coated copper grid, which was used as a TEM specimen.

Fourier transform infrared (FT-IR) spectroscopy was carried out on a Bruker VECTOR 22 spectrometer, with KBr pellet technique.

Diffuse reflectance UV–vis absorption spectroscopy was employed on a JASCO V-570 UV-V-NIR spectrophotometer over the wavelength range 300–1000 nm, using $BaSO_4$ as a reference.

X-ray photoelectron spectroscopy (XPS) measurements were performed on a Kratos Axis Ultra DLD (delay line detector) spectrometer equipped with a monochromatic Al K_α X-ray source (1486.6 eV). All XPS spectra were recorded using an aperture slot of 300 μm × 700 μm, survey spectra were recorded with a pass energy of 160 eV, and high resolution spectra with a pass energy of 40 eV.

2.3. Photocatalytic activity testing

The photocatalytic activity of the prepared N-doped titania catalysts was evaluated by the degradation of methylene orange (MO) dye under UV-light irradiation and Rhodamine B (RhB) dye under visible-light irradiation, respectively. In the MO degradation experiment, 5.5 mg of the catalyst powder was placed into a tubular quartz reactor of 100 ml of MO aqueous solution (1×10^{-5} mol/L), and a 125 W UV lamp with maximum emission at 365 nm located at 10 cm higher than the solution surrounded by a circulating water tube. The suspensions were magnetically stirred in the dark for 30 min to ensure the establishment of an adsorption/desorption equilibrium, and then exposed to the light irradiation at room temperature. At given time intervals, about 5 ml liquor was sampled, centrifuged for 5 min to discard any sediment. For the photodecomposition of RhB under visible light, the same above process was carried out with a household desktop lamp with a 40-W tungsten bulb as the visible-light source, of which the wavelength range is usually considered as 400–2500 nm, and the concentration of RhB solution and the amount of catalyst used are 1×10^{-5} mol/L and 20 mg, respectively. The absorbance of reaction solutions was measured using a SP-722 spectrometer at λ_{max} = 464 nm for MO and λ_{max} = 554 nm for RhB.

3. Results and discussion

3.1. SEM and TEM

The titania samples, prepared by the hydrolysis of tetrabutyl titanate in the absence of surfactant and autoclaving at 60–80 °C, are mainly tens to several tens of micrometers in size with irregular shapes, but with a macroporous structure. Fig. 1a and b are the SEM images of the MMTD samples prepared by

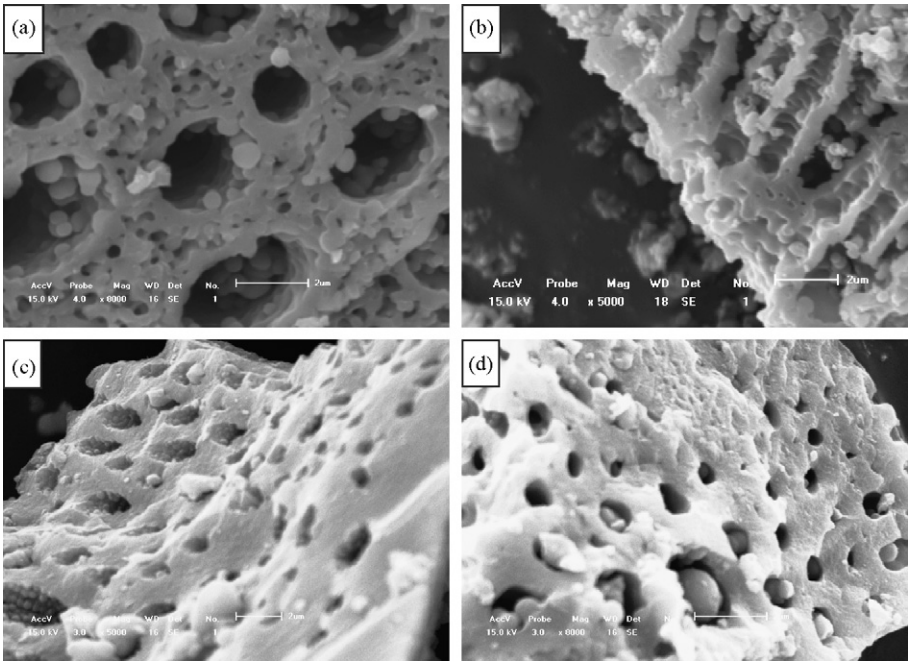

Fig. 1. SEM images of the MMTD material prepared at 60 °C (a and b) and its nitrogen-doping products: N-T-2/350 (c) and N-T-2/450 (d).

60 °C-autoclaving, showing the macroscopic network structure with macropores of 500–1000 nm in size. The macrochannels are arranged parallel to each other and perpendicular to the tangent of the surface of the particles, with the length of 2–8 μm; and the macroporous framework is composed by the assembly of small particles, leaving small holes in the macropore-walls of 300–800 nm in thickness. Since no surfactant or template participated in the synthesis, the macroporous structure of titanium dioxide formed spontaneously, as described previously in the spontaneous template-free assembly of ordered macroporous titania, alumina, aluminosilicate, titanium and zirconium phosphates [39–44]. Indeed, recent works have revealed that the surfactant molecules took almost no directing or templating role in the formation of macroporous structures, but significantly influenced the textural properties and the porous hierarchy [43,44]. The hydrolysis of Ti-alkoxide precursors in the acidic solution would result in the rapid formation of nanometer-sized titanium oxo clusters and titania particles, and a lot of butanol molecules were quickly and simultaneously generated by the hydrolysis reaction and polycondensation, which might produce microphase-separated domains of titania-based nanoparticles and water/alcohol channels that are the initiators and the driving force for the formation of the macrochannels [39,40,43]. The regular self-assembly of the nanoparticles, which would be consolidated during the autoclaving process, could create a network of mesoporous channels between the macrochannels.

After N-doping of this 60 °C-autoclaved MMTD sample, the well-defined macroporous structure can be retained (Fig. 1c and d). However, the surfaces of N-doped materials are smoother than MMTD, and the small holes in the macroporous walls between the macrochannels are unobserved, due to the possible solidification of the inorganic framework during the high-temperature treatment of 350–550 °C.

The fine particulate morphology between the macrochannels of both as-synthesized MMTD and N-doped titania materials is confirmed by the TEM images (Fig. 2). Fig. 2a and b is the TEM image of the as-synthesized MMTD, indicating the macropore walls are composed of nanoparticals with the size of tens nanometers, which present interparticle mesoporosity without long-range ordered mesostructure. Fig. 2c and d is the TEM image of the sample after nitridation, also revealing the wormhole-like mesopores in the macroporous frameworks resulted from the nanoparticle assembly.

It is clearly seen that such a hierarchical structure of uniform macrochannels with mesoporous walls of nanoparticle assembly self-formed during the synergistic packing of the nanoparticles and rapid release of alkanol molecules, and could retain during the nitridation process. It is noticeable that the autoclaving temperature may affect the hierarchical macrostructure of the MMTD materials. When the autoclaving temperature increased to 80 °C, an alternatively macroporous structure with smaller macropore size of 125–250 nm was obtained (Fig. 3), in which the small interconnected particles assembled too compactly to leave observable holes in the macropore-walls by conventional SEM. This indicates that the elevated autoclaving temperature resulted in different microphase separation process for the spontaneous formation of macroporous structure. However, considering that the macrochannels with the diameters close to the visible-light wavelength may serve as the light-transfer paths for introducing photoenergy into the interior of titania and is expected to increase the light utilization efficiency, the 60 °C-autoclaved MMTD sample and its N-doping production were then selected for further characterization and catalytic testing. Moreover, the stirring condition during the synthesis influenced significantly the macrostructure production. Under vigorous stirring, no macrochannels were observed, but

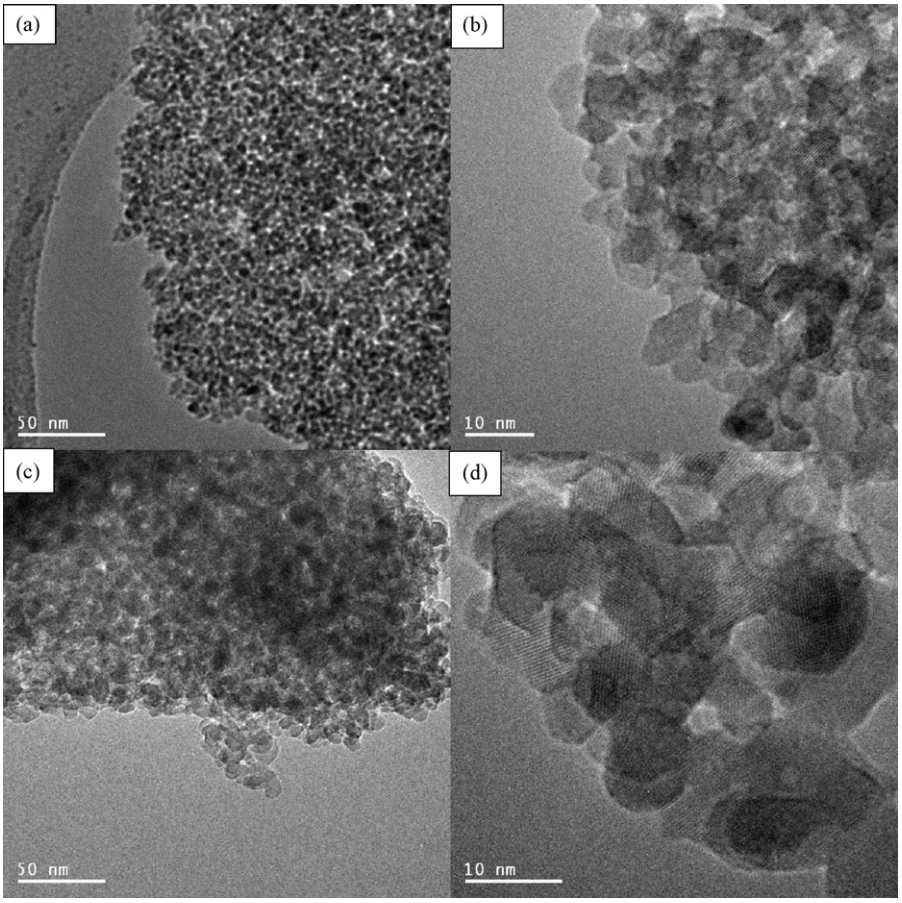

Fig. 2. TEM images of the (a and b) MMTD and (c and d) N-T-2/450 samples.

wormhole-like mesostructure was still obtained as revealed by the SEM and TEM images.

3.2. XRD and N_2 sorption analysis

Fig. 4 shows the XRD patterns of the as-synthesized MMTD and N-doped meso-macroporous titania. The samples after N-doping treatment showed a slight change of color from white to yellowish. From the XRD patterns, it was found that a bicrystalline structure (anatase and brookite) appears in the as-synthesized MMTD, and can retain in the N-doped samples. The phase contents of the samples can be calculated from the relative peak intensities of anatase (1 0 1) and brookite (1 2 1) peaks with the following formulas according to Zhang and Banfield [45]: $W_A = k_A A_A/(k_A A_A + A_R + k_B A_B)$, $W_R = A_R/(k_A A_A + A_R + k_B A_B)$, and $W_B = k_B A_B/(k_A A_A + A_R + k_B A_B)$, where W_A, W_R, and W_B represent the weight fractions of anatase, rutile, and brookite, respectively. A_A, A_R, and A_B are the integrated intensities of anatase (1 0 1), rutile (1 1 0), and brookite (1 2 1) peaks, respectively. The variables k_A and k_B are two coefficients, which were found to be 0.886 and 2.721, respectively [45]. The crystallite sizes of the resultant titania phases can be estimated by the Scherrer's formula [46]: $D_{(h\ k\ l)} = K_1\lambda/(\beta_{1/2} \cos\theta)$, where $D_{(h\ k\ l)}$ is the crystal size, K_1 is the factor of the crystal shape, λ is the wavelength of X-ray radiation (0.1548 nm for Cu K_α radiation), β is the full width at

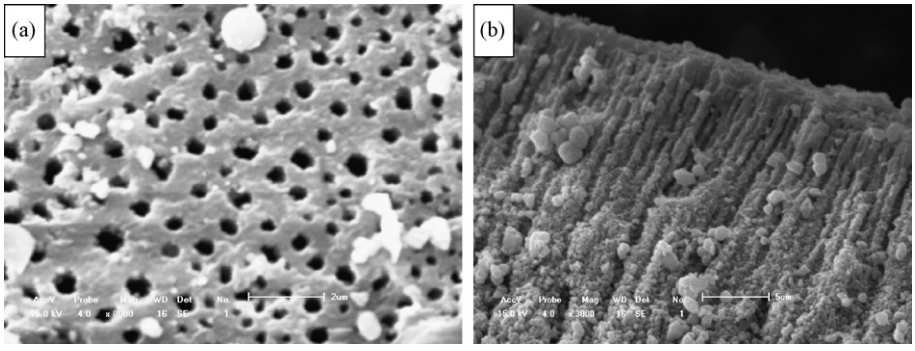

Fig. 3. SEM images of the MMTD materials prepared at 80 °C.

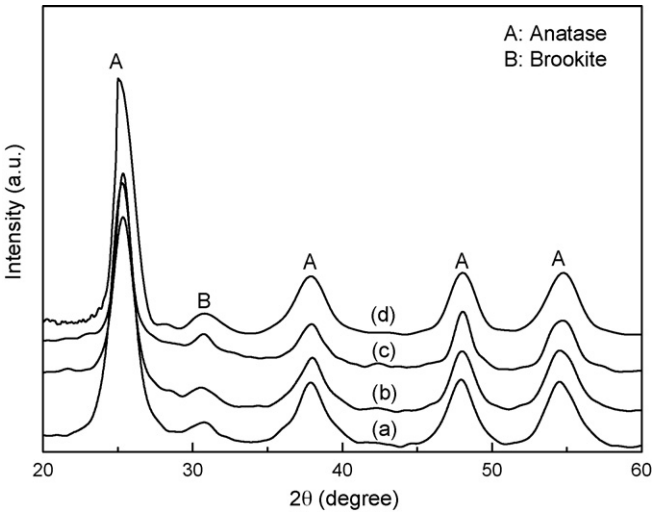

Fig. 4. XRD patterns of (a) the prepared MMTD sample and the nitridation products (b) N-T-2/350, (c) N-T-1/450 and (d) N-T-2/450.

half-maximum, and θ is the diffraction angle. The calculated phase contents of anatase and brookite, as well as the crystallite sizes, are shown in Table 1. It is seen that the crystallite size of anatase increased after N-doping, while the content of anatase decreased when the nitridation temperature or the urea content was low, but increased again when both the nitridation temperature and the urea content were high. The N-T-2/550 sample has the largest content of anatase. Previous work has demonstrated that the anatase phase has higher photoactivity than the other two titania phases [47], but lower than the mix-crystal titania structures with the optical concentration of anatase phase [48–50]. Our MMTD sample and its nitrogen-doping products have a bicrystalline framework dominated by the anatase phase, which may benefit their photocatalytic performance.

Fig. 5 shows the representative nitrogen adsorption–desorption isotherms and the corresponding pore size distributions of the as-synthesized MMTD and N-doped N-T-*x*/*y* samples. All isotherms are of type IV and characteristic of mesoporous materials, according to the IUPAC classification. A hysteresis loop with a triangular shape and a steep desorption branch is observed in the isotherms, which belongs to the type H2 hysteresis loop, suggesting the presence of pores with narrow mouths (ink-bottles-like pores) [51]. The pore size distribution is calculated by the BJH method from the adsorption branch of the isotherms. The textural properties of all samples are given in Table 1. The adsorption isotherm of as-synthesized MMTD exhibits a large increase in the P/P_0 range of 0.2–0.4. Correspondingly the pore size of the as-synthesized MMTD is centered at 2.2 nm with a high BET surface area of 280 m^2/g. This porosity should be as a result of the organized aggregation of titania nanoparticles arranged in a fairly uniform way that hydrolysis product of titanium *n*-alkoxide. After nitridation by heating with urea, the position of the inflection point in the isotherm of as-synthesized MMTD moved to higher P/P_0 range of 0.4–0.6, indicating the enlargement of the pore size. The pore sizes the N-doped samples increased with the nitridation temperature, accompanied with the decrease of BET surface areas and total pore volumes (Table 1). This should be the effect of the heating treatment during the N-doping.

3.3. FT-IR and XPS

FT-IR and XPS spectra are collected to study the surface chemistry of the photocatalysts. Fig. 6 shows the FT-IR spectra of N-T-*x*/*y* samples obtained with different urea concentration and calcination temperature. The broad absorption peaks around 3400 cm^{-1} and the band at 1630 cm^{-1} correspond to the surface adsorbed water and the hydroxyl groups. Low-frequency bands in the range $<500\ cm^{-1}$ correspond to the Ti–O–Ti vibration of the network [27,52]. Compared with the spectrum of pure titania (not shown), the N-T-*x*/*y* samples displayed several more peaks, such as 1129, 1196 and 1386 cm^{-1}. The bands of 1129 and 1196 cm^{-1} could be attributed to the nitrogen atoms embedded in the TiO_2 network in the form of O–Ti–N bonds [53]. The peak at 1386 cm^{-1} corresponds to the surface-adsorbed NH_3 molecules [53] or hyponitrite ions [54,55]. This indicates that the treatment of the MMTD precursor with urea resulted in not only the chemisorption of NH_3 molecules on the TiO_2 surface but also

Table 1
Summary of the physicochemical properties of the as-synthesized MMTD and N-doped titania samples

Material	Anatase		Brookite		S_{BET}[c] (m^2/g)	$D_{BJH\text{-}ads}$[d] (nm)	D_{ave}[e] (nm)	V_{pore}[f] (cm^3/g)
	Crystallite size[a] (nm)	Content[b] (%)	Crystallite size[a] (nm)	Content[b] (%)				
MMTD	10.2	89.5	6.8	10.5	280	2.2	3.3	0.23
N-T-2/350	13.9	86.8	5.1	13.2	183	2.4	4.3	0.20
N-T-1/450	13.9	84.2	6.8	15.8	116	5.4	5.6	0.16
N-T-2/450	14.8	90.7	4.1	9.3	121	5.4	5.2	0.16
N-T-2/550	15.2	91.2	4.1	8.8	87	6.8	7.2	0.13

[a] Calculated by the Scherrer's formula.
[b] Calculated using the formula in ref. [45].
[c] BET surface area calculated from the linear part of the BET plot.
[d] Estimated using the adsorption branch of the isotherm by the BJH method.
[e] Average pore size.
[f] Single point total pore volume of pores at $P/P_0 = 0.97$.

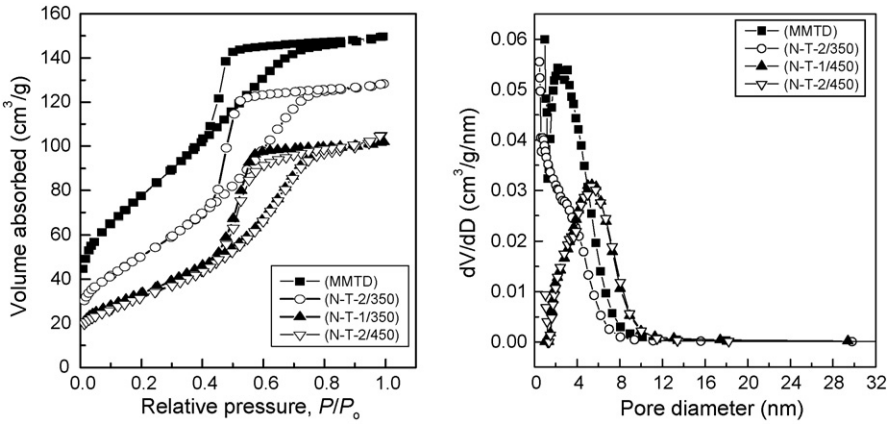

Fig. 5. (left) N_2 adsorption-desorption isotherms and (right) the corresponding BJH pore size distribution curves of the prepared samples.

the nitridation of the TiO_2 in network. Since no peaks appear at 1618, 1318 and 750 cm^{-1}, which are the typical infrared bands of NO_2, there is no possibility for significant formation and/or physisorption of NO_2 species on the surface of the monitored particles [56].

Fig. 7 shows the high-resolution XPS spectra of N 1s, Ti 2p and O 1s, taken on the surface of the N-T-1/450, N-T-2/450 samples. The peaks for Ti $2p_{3/2}$ and Ti $2p_{1/2}$ are situated at 458.6 and 464.4 eV for N-T-1/450 materials and 458.3 and 464.1 for N-T-2/450 materials, respectively. These binding energies are characteristic of Ti^{4+}. Compared with the binding energy of pure TiO_2 (459 eV for Ti $2p_{3/2}$ and 464.8 eV for Ti $2p_{1/2}$) [44], the binding energy of Ti 2p decreases after nitrogen doping, and moreover decreases with the increase of the urea concentration. This is the result from different electronic interactions of Ti with anions, which causes partial electron transformation from the N to the Ti and an increase of the electron density on Ti because of the lower electronegativity of nitrogen compared to oxygen [21], suggesting the nitrogen incorporates into the lattice and substitutes for oxygen. The O 1s signals at 529.9 eV for N-T-1/450 and 529.6 eV for N-T-2/450 are ascribed to the oxygen in Ti–O bond of TiO_2. A shoulder peak around 531.3 eV can be also observed, which might be assigned to the oxygen in titanium suboxides (such as TiO) [57] or Ti–N–O bonds [58]. Cong et al. [21] believed that the chemical states of the N-doped into TiO_2 might be various and coexist in the form of N–Ti–O and Ti–O–N.

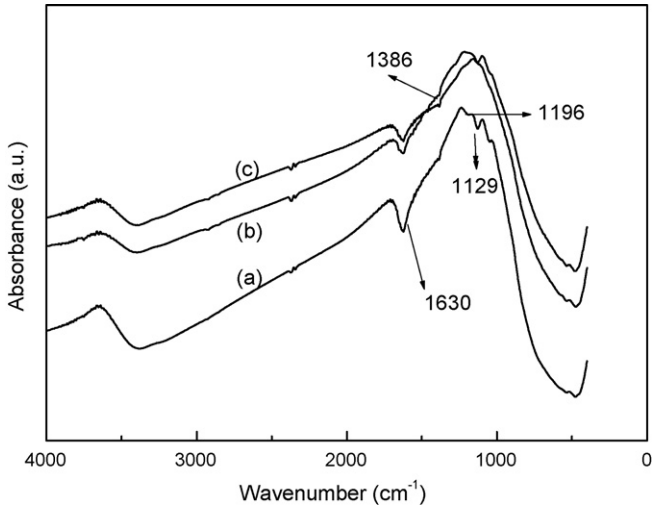

Fig. 6. The FT-IR spectra of the N-doped TiO_2 materials: (a) N-T-2/350, (b) N-T-1/450 and (c) N-T-2/450.

The N 1s spectrum can be deconvoluted into a main component at 399–400 eV with a shoulder at 401.5 eV. Although the assignment of the XPS peak of N1s has still been under debate, the observed N 1s spectra of our N-T-*x*/*y* samples are in the range of previously reported N-doped titanium dioxide [21,55,59–61]. The main peak of 399–400 eV might be attributed to the anionic N^- in O–Ti–N linkages, though this line was attributed to adsorbed molecular nitrogen in some literature [58,62]. The binding energy of this peak is higher than that of TiN appeared at $\leq$397.5 eV [63], and lower than that of hyponitrite type nitrogen at 404 eV [55]. This indicates the different nitrogen environment, resulted from the N-doping into the TiO_2 lattice that reduces the electron density on the nitrogen due to the high electronegativity of oxygen [21]. Valentin et al. [64] observed N 1s core level at 400 eV and attributed it to a lower valence state of nitrogen. Gole et al. [60] and Chen and Burda [61] observed the N 1s level at 401.3 eV and considered it to be N–Ti–O linkage in the lattice. Thus, the presence of N 1s shoulder peak due to the formation of N–Ti–O bonds, and the observed Ti $2p_{3/2}$ level at ~458.3 eV, can ascertain a considerable modification of the lattice due to N substitution in these meso-macroporous titania materials. The contents of nitrogen atoms in the N-T-1/450 and N-T-2/450 samples are estimated to be 0.74 and 1.43%, respectively, from the XPS results.

3.4. UV–vis spectroscopy

Fig. 8 shows the UV–vis diffuse reflectance spectra of the MMTD and the N-T-*x*/*y* materials. The MMTD sample showed a single sharp edge with the band gap absorption onset at 395 nm, while the N-T-*x*/*y* showed two absorption edges: the main edge due to the oxide at 400–406 nm and a weak shoulder due to nitrogen doping at 400–500 nm. Noticeable shifts of the absorbance shoulder to the visible-light region correspond to the observed yellow-colored feature in the meso-macroporous

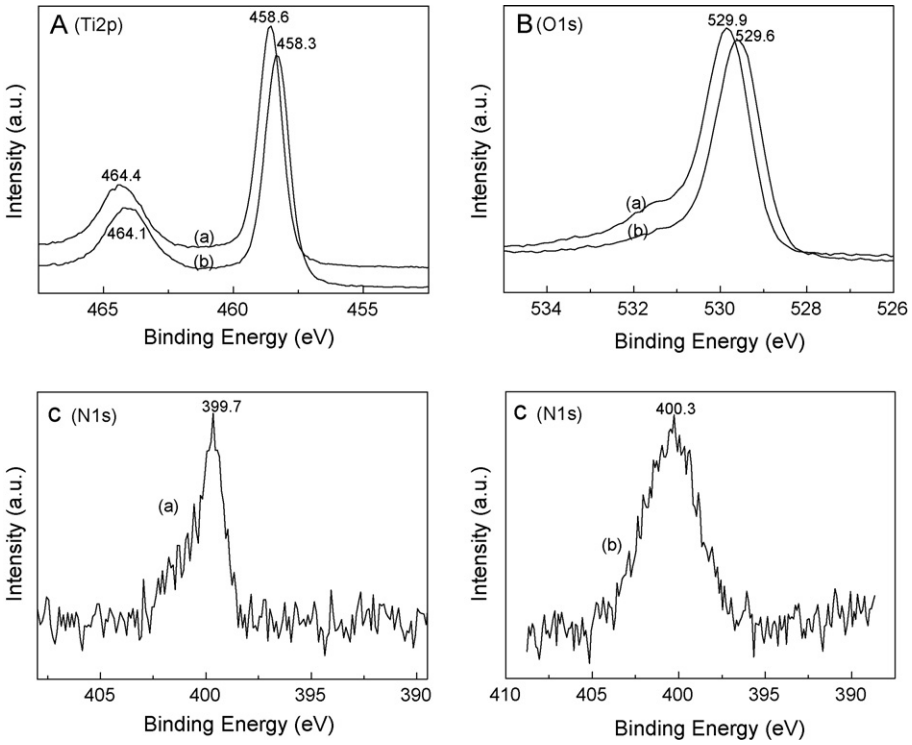

Fig. 7. (A) Ti 2p, (B) O 1s and (C) N 1s XPS spectra of the N-doped meso-macroporous titania samples: (a) N-T-1/450 and (b) N-T-2/450.

$TiO_{2-x}N_x$ samples. Furthermore, the absorption onset of this shoulder peak shifts toward the lower energy region with the increase of nitrogen content in the N-T-*x*/*y*, indicating the N-T-*x*/*y* samples sensitive to visible light. The absorbance shoulders heightened with the increase of x value for $TiO_{2-x}N_x$. This shoulder peak should be responsible for the visible-light catalytic activity as discussed below.

The bandgap of the as-synthesized MMTD is 3.14 eV, calculated by the formula [65] $E_g = 1240/\lambda_g$, where the λ_g is the wavelength value corresponding to the intersection point of the vertical and horizontal parts of the spectra. This bandgap of MMTD is lower than that of the commercial white TiO_2 (3.2 eV). After N-doping, two bandgaps of 3.05–3.10 and 2.54–2.48 eV are obtained (Table 2). The first bandgap of N-T-*x*/*y* is lower than that of the MMTD material (3.14 eV), which reflects the effect of N-doping on the main band edges of the oxides. The second gaps suggest again that nitrogen doping contributed to the red shift for the bandgap narrowing, due to the occurrence of some electronic structure modification during nitridation. This significant narrowing of the band gaps and the visible-light absorbance of N-T-*x*/*y* materials are of great importance for their practical applications since they could be active even by sunlight.

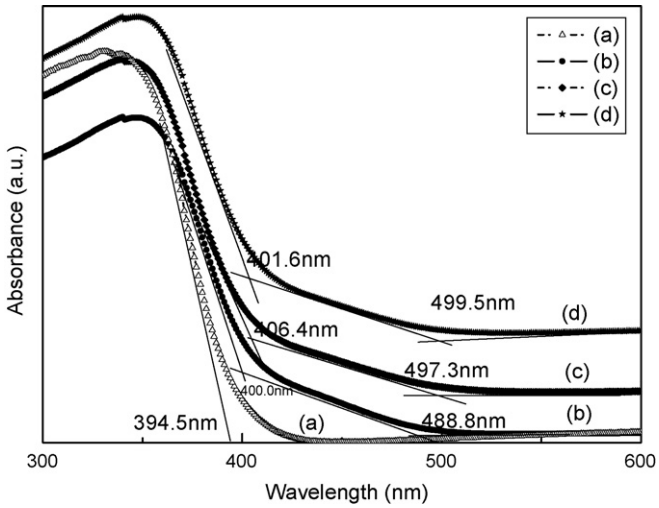

Fig. 8. The UV–vis diffuse reflectance spectra of the prepared MMTD and N-doped TiO_2: (a) MMTD, (b) N-T-2/350, (c) N-T-1/450 and (d) N-T-2/450.

3.5. Photocatalytic activity

To get insight into the effect of N-doping on the photocatalytic properties of the prepared meso-macroporous photocatalysts, the degradation of MO aqueous solution under UV irradiation and the degradation of RhB aqueous solution under visible-light irradiation were carried out, and compared with that of undoped MMTD (Fig. 9). The photodegradation mechanism of MO and RhB dyes has been well discussed in the literature [26,53], which might be that upon excitation, a conduction-band electron and a valence-band hole separate, and then the hole initiates an oxidative reaction while the electron initiates a reductive reaction. Organic compounds, such as MO or RhB, are believed to be destroyed through direct oxidation by the trapped holes or attack by hydroxyl groups. For comparison, a blank experiment (self-photosensitized process) was performed in the absence of any catalysts, and only a very small degree of photodegradation took place under any light irradiation. As shown in Fig. 9A, a big degree of

Table 2
Nitrogen content, band gap value and photodegradation rate of dye molecules

Sample	N content (%)	Bandgap (eV)	Degradation rate of MO	Degradation rate of RhB
MMTD	0	3.14	5.4×10^{-3}	3.7×10^{-3}
N-T-2/350	–	3.10, 2.54	7.4×10^{-3}	4.0×10^{-3}
N-T-1/450	0.74	3.05, 2.49	1.03×10^{-2}	4.0×10^{-3}
N-T-2/450	1.43	3.09, 2.48	2.32×10^{-2}	5.3×10^{-3}
N-T-2/550	–	–	1.5×10^{-2}	4.7×10^{-3}

photodegradation of MO occurred under UV irradiation. It can be seen that MMTD exhibits a good UV-photocatalytic activity, but the N-doping enhances its photocatalytic activity remarkably. With the increase of urea concentration during N-doping process, the photocatalytic activities of the resultant N-T-*x*/*y* samples considerably increase. After 210 min of UV irradiation, MO was to be degraded 44, 71, 83.5, 90 and nearly 100% for no catalyst, MMTD, N-T-2/350, N-T-1/450, and N-T-2/450, respectively. While the activity of N-T-2/550 was a little lower than that of N-T-2/450, which may be due to the lower surface area and pore volume in N-T-2/550 after higher temperature calcination. The optimum reactivity is observed in the N-T-2/450 sample.

Under visible-light irradiation, as shown in Fig. 9B, a distinct degradation of RhB occurred in the presence of the N-T-*x*/*y* samples. The content of RhB decreased quickly with the prolonging of the irradiation time. The sequence of visible-light photocatalytic activity of the obtained catalysts is same to that under UV irradiation, giving the following: N-T-2/450 > N-T-2/550 > N-T-1/450 > N-T-2/350 > MMTD > no catalyst, with the degradation of 44.9, 40.5, 36.9, 36.3, 34.8 and 1.5% after only 100 min of visible-light irradiation, respectively.

The photocatalytic degradation reaction can be assumed to follow a pseudo-first-order expression: $\ln(C_0/C) = kt$, where C_0/C is the normalized organic compounds concentration and k is the apparent reaction rate (min^{-1}). Fig. 9C and D shows the relationship between $\ln(C_0/C)$ and the irradiation time (t) for the UV degradation of MO and the visible-light degradation of RhB, respectively. The photocatalytic activity has been defined as the overall degradation rate constant of the catalysts. By plotting $\ln(C_0/C)$ as a function of irradiation time through regression, we obtained for each catalyst sample the k (min^{-1}) constant from the slopes of the simulated straight lines. All the curves can be fitted roughly to a straight line, and the pseudo-first-order reaction rate constants (k) are listed in Table 2. It is apparently shown that the UV degradation rate constant of MO

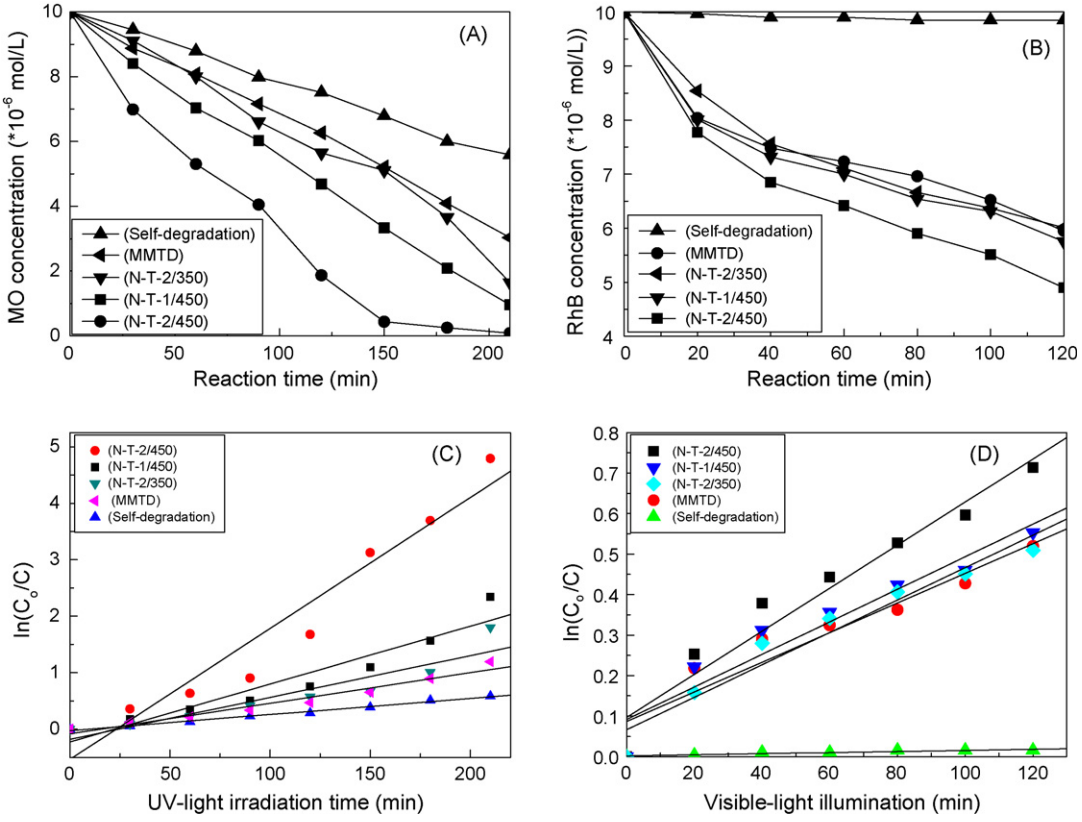

Fig. 9. (A) The residual concentration of MO solution after UV photodecomposition by MMTD and N-T-*x*/*y* catalysts, (B) the residual concentration of RhB solution after visible light photodecomposition by MMTD and N-T-*x*/*y* catalysts; (C and D) a plot of $\ln(C_0/C)$ versus the irradiation time from (A and B), respectively, showing the fitting results using the pseudo-first-order reaction.

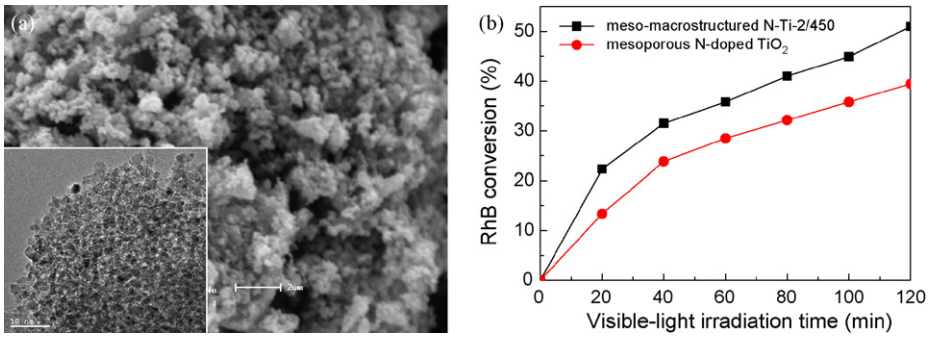

Fig. 10. (a) SEM and TEM (inset) images of the mesoporous N-doped TiO_2 without macrochannels nitrided at 450 °C and (b) the conversion of RhB under visible-light irradiation for the N-T-2/450 catalysts with and without macrostructure.

increased from 5.4×10^{-3} to 2.32×10^{-2} by nitridation of MMTD, and the visible-light degradation rate constant of RhB increased from 3.7×10^{-3} to 5.3×10^{-3}, which is consistent to the bandgap narrowing. The photocatalytic results clearly indicate that the nitrogen doping can effectively improve the photocatalytic activity in both the UV and visible-light region.

The mesoporous N-doped TiO_2 catalyst without macrochannels was also prepared by the same procedure as N-T-2/450 except with vigorous stirring in the synthesis of mesoporous titania precursor (Fig. 10a), which has a surface area of 133 m^2/g with mesopore size of 5.6 nm, and its photocatalytic activity was tested under visible-light irradiation (Fig. 10b). The comparison in Fig. 10b of the photocatalytic activities between the catalysts with meso-macroporous structure and with only mesoporous structure shows a 12.4% drop in photocatalytic activity (after 120-min-irradiation) for the absence of light-penetrationg and molecular-diffusing macrochannels. This indicates clearly the beneficial effects of macrochannels.

4. Conclusions

Hierarchically meso-macroporous titania with a bicrystalline (anatase and brookite) framework was prepared by a simple template-free method of nanoparticle assembly process. Nitridation of the as-prepared MMTD with the use of urea as a nitrogen donor resulted in the formation of meso-macroporous $TiO_{2-x}N_x$ materials, with the retaining of the hierarchical porosity, high surface area and bicrystalline structure. The obtained MMTD and N-T-*x*/*y* samples possess the macrochannels with the size of 500–1000 nm, and the macroporous framework is composed of accessible mesochannels with a wormhole-like array, which benefit to their photocatalytic performance. The N-substitution into the lattice of MMTD through the formation of N–Ti–O bonds was confirmed by the FT-IR, XPS and UV–vis spectroscopy. A red-shift of the absorption edge from 387 to nearly 500 nm was observed after N-doping, resulting in bandgap reducing to 2.48 eV. The MMTD showed a good photocatalytic activity in the degradation of dye molecules, while the photocatalytic activities of nitrogen-doped samples were significantly improved with an increase of the actual nitrogen doping concentration. The efficiency of the photocatalytic degradation of MO under UV irradiation, as well as in the photodegradation of RhB under visible-light irradiation, on the N-T-*x*/*y* samples is much better than that of the MMTD.

Acknowledgements

This work was supported by the National Natural Science Foundation of China (20473041, 20673060), the National Basic Research Program of China (2003CB615801), the Specialized Research Fund for the Doctoral Program of Higher Education (20070055014), the Program for New Century Excellent Talents in University (NCET-06-0215) and Nankai University.

References

[1] A. Fujishima, K. Hashimoto, T. Watanabe, TiO_2 Photocatalysis, Bkc, Inc., Tokyo, Japan, 1999.
[2] D.E. Ollis, H. Al-Ekabi, Photocatalytic Purification and Treatment of Water and Air, Elsevier, Amsterdam, 1993.
[3] M.R. Hoffmann, S.T. Martin, W. Choi, D.W. Bahnemann, Environmental applications of semiconductor photocatalysis, Chem. Rev. 95 (1995) 69–96.
[4] S. Sato, Photocatalytic activity of nitrogen oxide (NO_x)-doped titanium dioxide in the visible region, Chem. Phys. Lett. 123 (1986) 126–128.
[5] R. Asahi, T. Morikawa, T. Ohwaki, K. Aoki, Y. Tage, Visible-light photocatalysis in nitrogen-doped titanium oxides, Science 293 (2001) 269–271.
[6] S. Sakthivel, H. Kisch, Photocatalytic and photoelectrochemical properties of nitrogen-doped titanium dioxide, Chem. Phys. Chem. 4 (2003) 487–490.
[7] M. Shen, Z. Wu, H. Huang, Y. Du, P. Yang, Carbon-doped anatase TiO_2 obtained from TiC for photocatalysis under visible light irradiation, Mater. Lett. 60 (2006) 693–697.
[8] J.C. Yu, W. Ho, J.G. Yu, H. Yip, P.K. Wong, J.C. Zhao, Efficient visible-light-induced photocatalytic disinfection on sulfur-doped nanocrystalline titania, Environ. Sci. Tech. 39 (2005) 1175–1179.
[9] W. Ho, J.C. Yu, S. Lee, Synthesis of hierarchical nanoporous F-doped TiO_2 spheres with visible light photocatalytic activity, Chem. Commun. (2006) 1115–1117.
[10] L. Lin, W. Lin, J.L. Xie, Y.X. Zhu, B.Y. Zhao, Y.C. Xie, Photocatalytic properties of phosphor-doped titania nanoparticles, Appl. Catal. B: Environ. 75 (2007) 52–58.
[11] X.T. Hong, Z.P. Wang, W.M. Cai, F. Lu, J. Zhang, Y.Z. Yang, N. Ma, Y.J. Liu, Visible-light-activated nanoparticle photocatalyst of iodine-doped titanium dioxide, Chem. Mater. 17 (2005) 1548–1552.
[12] Y. Wang, Z.H. Jiang, F.J. Yang, Effect of Fe-doping on the pore structure of mesoporous titania, Mater. Sci. Eng. B 134 (2006) 76–79.

[13] A. Ghicov, B. Schmidt, J. Kunze, P. Schmuki, Photoresponse in the visible range from Cr doped TiO_2 nanotubes, Chem. Phys. Lett. 433 (2007) 323–326.
[14] K. Zhang, W. Xu, X. Li, S. Zheng, G. Xu, Effect of dopant concentration on photocatalytic activity of TiO_2 film doped by Mn non-uniformly, Cent. Eur. J. Chem. 4 (2006) 234–245.
[15] Y.H. Xu, H.R. Chen, Z.X. Zeng, B. Lei, Investigation on mechanism of photocatalytic activity enhancement of nanometer cerium-doped titania, Appl. Surf. Sci. 252 (2006) 8565–8570.
[16] H. Yu, X.J. Li, S.J. Zheng, W. Xu, Photocatalytic activity of TiO_2 thin film non-uniformly doped by Ni, Mater. Chem. Phys. 97 (2006) 59–63.
[17] D. Li, H. Haneda, S. Hishita, N. Ohashi, Visible-light-driven N-F-co-doped TiO_2 photocatalysts. 1. Synthesis by spray pyrolysis and surface characterization, Chem. Mater. 17 (2005) 2588–2595.
[18] H. Sun, Y. Bai, Y. Cheng, W. Jin, N. Xu, Preparation and characterization of visible-light-driven carbon-sulfur-codoped TiO_2 photocatalysts, Ind. Eng. Chem. Res. 45 (2006) 4971–4976.
[19] D. Chen, Z. Jiang, J. Geng, Q. Wang, D. Yang, Carbon and nitrogen co-doped TiO_2 with enhanced visible-light photocatalytic activity, Ind. Eng. Chem. Res. 46 (2007) 2741–2746.
[20] S. Yin, Y. Aita, M. Komatsu, T. Sato, Visible-light-induced photocatalytic activity of $TiO_{2-x}N_y$ prepared by solvothermal process in urea–alcohol system, J. Eur. Ceram. Soc. 26 (2006) 2735–2742.
[21] Y. Cong, J. Zhang, F. Chen, M. Anpo, Synthesis and characterization of nitrogen-doped TiO_2 nanophotocatalyst with high visible light activity, J. Phys. Chem. C 111 (2007) 6976–6982.
[22] Y. Nosaka, M. Matsushita, J. Nishino, A.Y. Nosaka, Nitrogen-doped titanium dioxide photocatalysts for visible response prepared by using organic compounds, Sci. Technol. Adv. Mater. 6 (2005) 143–148.
[23] S. Sato, R. Nakamura, S. Abe, Visible-light sensitization of TiO_2 photocatalysts by wet-method N doping, Appl. Catal. A: Gen. 284 (2005) 131–137.
[24] Y. Yue, Z. Gao, Synthesis of mesoporous TiO_2 with a crystalline framework, Chem. Commun. (2000) 1755–1756.
[25] J.C. Yu, L. Zhang, J. Yu, Direct sonochemical preparation and characterization of highly active mesoporous TiO_2 with a bicrystalline framework, Chem. Mater. 14 (2002) 4647–4653.
[26] H. Luo, C. Wang, Y. Yan, Synthesis of mesostructured titania with controlled crystalline framework, Chem. Mater. 15 (2003) 3841–3846.
[27] T. Peng, D. Zhao, K. Dai, W. Shi, K. Hirao, Synthesis of tianium dioxide nanoparticles with mesoporous anatase wall and high photocatalytic activity, J. Phys. Chem. B 109 (2005) 4947–4952.
[28] Q. Sheng, Y. Cong, S. Yuan, J. Zhang, M. Anpo, Synthesis of bi-porous TiO_2 with crystalline framework using a double surfactant system, Microporous Mesoporous Mater. 95 (2006) 220–225.
[29] G. Liu, Z. Chen, C. Dong, Y. Zhao, F. Li, G.Q. Lu, H.M. Cheng, Visible light photocatalyst: iodine-doped mesoporous titania with a bicrystalline framework, J. Phys. Chem. B 110 (2006) 20823–20828.
[30] S. Yuan, Q. Sheng, J. Zhang, F. Chen, M. Anpo, Q. Zhang, Synthesis of La^{3+} doped mesoporous titania with highly crystallized walls, Microporous Mesoporous Mater. 79 (2005) 93–99.
[31] W. Yao, H. Fang, E. Ou, J. Wang, Z. Yan, Highly efficient catalytic oxidation of cyclohexane over cobalt-doped mesoporous titania with anatase crystalline structure, Catal. Commun. 7 (2006) 387–390.
[32] Z.Y. Yuan, B.L. Su, Insights into hierarchically meso-macroporous structured materials, J. Mater. Chem. 16 (2006) 663–677.
[33] P. Yang, T. Deng, D. Zhao, P. Feng, D. Pine, B.F. Chmelka, G.M. Whitesides, G.D. Stucky, Hierarchically ordered oxides, Science 282 (1998) 2244–2246.
[34] D. Grosso, G.J.D.A.S. Illia, E.L. Crepaldi, B. Charleux, C. Sanchez, Nanocrystalline transition-metal oxide spheres with controlled multi-scale porosity, Adv. Funct. Mater. 13 (2003) 37–42.
[35] Z.Y. Yuan, T.Z. Ren, B.L. Su, Hierarchically mesostructured titania materials with an unusual interior macroporous structure, Adv. Mater. 15 (2003) 1462–1465.
[36] M. Iwasaki, S.A. Davis, S. Mann, Spongelike macroporous TiO_2 monoliths prepared from starch gel template, J. Sol–Gel Sci. Tech. 32 (2004) 99–105.
[37] H. Maekawa, J. Esquena, S. Bishop, C. Solans, B.F. Chmelka, Meso/macroporous inorganic oxide monoliths from polymer foams, Adv. Mater. 15 (2003) 591–596.
[38] X. Wang, J.C. Yu, C. Ho, Y. Hou, X. Fu, Photocatalytic activity of a hierarchically macro/mesoporous titania, Langmuir 21 (2005) 2552–2559.
[39] A. Collins, D. Carriazo, S.A. Davis, S. Mann, Spontaneous template-free assembly of ordered macroporous titania, Chem. Commun. (2004) 568–569.
[40] T.Z. Ren, Z.Y. Yuan, B.L. Su, Thermally stable macroporous zirconium phosphates with supermicroporous walls: a self-formation phenomenon of hierarchy, Chem. Commun. (2004) 2730–2731.
[41] W. Deng, B.H. Shanks, Synthesis of hierarchically structured aluminas under controlled hydrodynamic conditions, Chem. Mater. 17 (2005) 3092–3100.
[42] A. Leonard, B.L. Su, A novel and template-free method for the spontaneous formation of aluminosilicate macro-channels with mesoporous walls, Chem. Commun. (2004) 1674–1675.
[43] Z.Y. Yuan, T.Z. Ren, A. Azioune, J.J. Pireaux, B.L. Su, Self-assembly of hierarchically mesoporous-macroporous phosphated nanocrystalline aluminum (oxyhydr)oxide materials, Chem. Mater. 18 (2006) 1753–1767.
[44] T.Z. Ren, Z.Y. Yuan, A. Azioune, J.J. Pireaux, B.L. Su, Tailoring the porous hierarchy of titanium phosphates, Langmuir 22 (2006) 3886–3894.
[45] H. Zhang, J.F. Banfield, Understanding polymorphic phase transformation behavior during growth of nanocrystalline aggregates: insights from TiO_2, J. Phys. Chem. B 104 (2000) 3481–3487.
[46] H.P. Klug, L.E. Alexander, X-ray Diffraction Procedure for Polycrystalline and Amorphous Materials, second ed., Wiley, New York, 1974.
[47] C. Adán, A. Bahamonde, M. Fernández-García, A. Martínez-Arias, Structure and activity of nanosized iron-doped anatase TiO_2 catalysts for phenol photocatalytic degradation, Appl. Catal. B: Environ. 72 (2007) 11–17.
[48] X.J. Ye, D. Chen, K.Y. Li, V. Shah, Photocatalytic oxidation of aldehydes/PCE using porous anatase titania and visible-light-responsive brookite titania, Chem. Eng. Commun. 194 (2007) 368–381.
[49] S.S. Yan, L.D. Wu, F. Chen, J.L. Zhang, Low-temperature preparation and characterization of TiO_2 thin films with a bicrystalline framework, Acta Physico-Chim. Sin. 23 (2007) 414–418.
[50] L.J. Zhou, S.S. Yan, B.Z. Tian, F. Chen, J.L. Zhang, J.Z. Huang, Preparation and characterization of anatase-brookite TiO_2 film on the PET surface, Acta Physico-Chim. Sin. 22 (2006) 569–573.
[51] M. Kruk, M. Jaroniec, Gas adsorption characterization of ordered organic-inorganic nanocomposite materials, Chem. Mater. 13 (2001) 3169–3183.
[52] G.J.A.A. Soler-Illia, A. Louis, C. Sanchez, Synthesis and characterization of mesostructured titania-based materials through evaporation-induced self-assembly, Chem. Mater. 14 (2002) 750–759.
[53] H. Li, J. Li, Y. Huo, Highly active TiO_2N photocatalysts prepared by treating TiO_2 precursors in NH_3/ethanol fluid under supercritical conditions, J. Phys. Chem. B 110 (2006) 1559–1565.
[54] J.A. Navio, C. Cerrillos, C. Real, Photo-induced transformation upon UV illumination in air of hyponitrite species $N_2O_2^{2-}$ preadsorbed on TiO_2 surface, Surf. Interface Anal. 24 (1996) 355–359.
[55] S. Sakthivel, M. Janczarek, H. Kisch, Visible light activity and photoelectrochemical properties of nitrogen-doped TiO_2, J. Phys. Chem. B 108 (2004) 19384–19387.
[56] X. Chen, Y. Lou, A.C.S. Samia, C. Burda, J.L. Gole, Formation of oxynitride as the photocatalytic enhancing site in nitrogen-doped titania nanocatalysts: comparison to a commercial nanopowder, Adv. Funct. Mater. 15 (2005) 41–49.
[57] G. Lu, S.L. Bernasek, J. Schwartz, Oxidation of a polycrystalline titanium surface by oxygen and water, Surf. Sci. 458 (2000) 80–90.
[58] E. György, A. Pérez del Pino, P. Serra, J.L. Morenza, Depth profiling characterisation of the surface layer obtained by pulsed Nd:YAG laser irradiation of titanium in nitrogen, Surf. Coat. Technol. 173 (2003) 265–270.
[59] R. Nakamura, T. Tanaka, Y. Nakato, Mechanism for visible light responses in anodic photocurrents at N-doped TiO_2 film electrodes, J. Phys. Chem. B 108 (2004) 10617–10620.

[60] J.L. Gole, J.D. Stout, C. Burda, Y. Lou, X. Chen, Highly efficient formation of visible light tunable $TiO_{2-x}N_x$ photocatalysts and their transformation at the nanoscale, J. Phys. Chem. B 108 (2004) 1230.

[61] X. Chen, C. Burda, Photoelectron spectroscopic investigation of nitrogen-doped titania nanoparticles, J. Phys. Chem. B 108 (2004) 15446–15449.

[62] G.A. Battiston, R. Gerbasi, A. Gregori, M. Porchia, S. Cattarin, G.A. Rizzi, PECVD of amorphous TiO_2 thin films: effect of growth temperature and plasma gas composition, Thin Solid Films 371 (2000) 126–131.

[63] N.C. Saha, H.G. Tompkins, Titanium nitride oxidation chemistry: an X-ray photoelectron spectroscopy study, J. Appl. Phys. 72 (1992) 3072–3079.

[64] C.D. Valentin, G. Pacchioni, A. Selloni, S. Livraghi, E. Giamello, Characterization of paramagnetic species in N-doped TiO_2 powders by EPR spectroscopy and DFT calculations, J. Phys. Chem. B 109 (2005) 11414–11419.

[65] L. Kõrösi, I. Dékány, Preparation and investigation of structural and photocatalytic properties of phosphate modified titanium dioxide, Colloids Surf. A 280 (2006) 146–154.